Innovative: International Multi-disciplinary Journal of Applied Technology
(ISSN 2995-486X) VOLUME 04 ISSUE 04, 2026

SPATIALLY RESOLVED COMPOSITE RADIOLOGICAL AND HEAVY METAL RISK ASSESSMENT AROUND THE ARIARIA MUNICIPAL WASTE DUMPSITE: BUFFER ZONE HAZARD MAPPING AND POPULATION EXPOSURE ANALYSIS IN NIGERIA

Gbarato, O. L.
Department of Physics, Ignatius Ajuru University of Education, Rivers State, Nigeria
oliver.gbarato@iaue.edu.ng

Ikata, E. S.
Department of Physics, Ignatius Ajuru University of Education, Rivers State, Nigeria

Nwi, A. A.
Department of Physics, Ignatius Ajuru University of Education, Rivers State, Nigeria

Abstract:
Municipal waste dumpsites in low- and middle-income countries are often unlined and poorly regulated, releasing a complex mixture of heavy metals and naturally occurring radionuclides into surrounding environments. Conventional risk assessments typically evaluate these hazards independently, thereby underestimating cumulative exposure and associated health risks. There is an urgent need for spatially explicit, integrated risk mapping approaches to inform effective intervention strategies. A field-based assessment was conducted around the ariaria dumpsite, Nigeria, using three concentric buffer zones (0–100 m, 100–300 m, and 300–500 m). Data collection included (i) in situ background ionizing radiation (BIR) measurements (n = 120) using a calibrated dosimeter, (ii) soil sampling (n = 45) for heavy metal analysis (Pb, Cd, Cr, As, Ni) via ICP-MS, and (iii) groundwater sampling (n = 15). Radiological indices (AEDE, ELCR) and toxicological indices (HQ, HI, CR) were computed. Spatial distributions were generated using ordinary kriging, and a Composite Risk Index (CRI = normalized AEDE + normalized HI + normalized CR) was developed. Population exposure was estimated through GIS-based overlay with high-resolution census data. BIR decreased from 0.21 μSv/h (0-100 m) to 0.09 μSv/h (300-500 m), while Pb concentrations declined from 85 mg/kg to 22 mg/kg, indicating consistent spatial attenuation. The CRI exceeded unity up to ~250 m from the dumpsite. Within the 0–100 m zone, approximately 1,250 residents are exposed to CRI > 1, corresponding to ELCR > 10^{-4} and HI >1. A significant spatial correlation between radiological and toxicological hazards (R^2 = 0.68, $p < 0.01$) suggests common waste sources. It was concluded that integrated spatial risk assessment reveals that single-hazard approaches underestimate environmental exposure. Similarly, the buffer zone framework provides

actionable guidance for resettlement and remediation, while the composite mapping approach offers a transferable tool for global dumpsite risk evaluation.

Keywords: Composite Risk Index; Dumpsite contamination; Heavy metals; Radiological risk; GIS mapping; Environmental health risk

Introduction

Rapid urbanisation and population growth in low- and middle-income countries have led to a sharp increase in municipal solid waste generation, outpacing the development of adequate waste management infrastructure. Reports by the United Nations Environment Programme and the World Bank consistently highlight the widespread reliance on open and uncontrolled dumpsites across sub-Saharan Africa, where formal sanitary landfills remain limited [1]. These sites typically receive heterogeneous waste streams, including municipal refuse, industrial by-products, medical waste, and electronic scrap, without engineered containment systems such as liners or leachate collection networks. As a result, they function as long-term, unregulated sources of environmental contamination [2].

A growing body of literature has documented elevated concentrations of heavy metals and naturally occurring radionuclides in soils, surface water, and groundwater surrounding such dumpsites. Studies across Nigeria and other parts of West Africa report significant enrichment of toxic elements such as lead, cadmium, chromium, and zinc, often exceeding international safety thresholds [3]. Similarly, radiological investigations have identified increased levels of radionuclides such as ^{226}Ra, ^{232}Th, and ^{40}K, contributing to enhanced background ionizing radiation (BIR) and elevated dose rates in waste-impacted environments [4]. These findings underscore the role of uncontrolled dumpsites as complex, multi-hazard systems with both chemical and radiological dimensions [5].

Despite the coexistence of multiple contaminants in dumpsite environments, most environmental risk assessments remain narrowly focused on a single class of hazard. Radiological studies typically employ gamma spectrometry or in situ survey methods to estimate absorbed dose rates, annual effective dose equivalent (AEDE), and excess lifetime cancer risk (ELCR), while heavy metal studies rely on toxicological frameworks such as those developed by the United States Environmental Protection Agency to evaluate hazard quotients (HQ), hazard indices (HI), and carcinogenic risks (CR). While each approach provides valuable insights, their separation creates an incomplete representation of environmental risk [6].

This siloed methodology overlooks several critical realities. First, it neglects the potential for synergistic or additive effects arising from simultaneous exposure to chemical and radiological stressors [7]. Second, it fails to account for shared exposure pathways, including ingestion of contaminated soil and water, inhalation of dust, and dermal contact. Third, it ignores the fact that both radionuclides and heavy metals originate from the same heterogeneous waste matrix and are mobilised through similar physical and geochemical processes, including advection, diffusion, sorption, and leaching [8]. Consequently, regulatory decisions based on single-hazard assessments may significantly underestimate the total environmental and public health burden experienced by communities living near dumpsites.

Recent advances in geographic information systems (GIS) have enabled the spatial mapping of environmental contaminants, offering improved visualization of pollution gradients and hotspot identification. A limited number of studies have attempted multi-pollutant mapping by integrating datasets on heavy metals and radiological parameters [9]. However, these efforts are often descriptive and stop short of translating spatial patterns into actionable risk metrics.

In particular, there remains a lack of studies that define practical buffer zones around dumpsites and

systematically evaluate how risk decays with distance, an approach that is directly relevant for land-use planning, zoning regulations, and potential resettlement decisions. Critically, there is no established methodology that simultaneously: (a) quantifies radiological and toxicological risks on a unified spatial grid; (b) develops a composite risk index that integrates multiple hazard types; (c) overlays population data to estimate the number of individuals exposed above safety thresholds; and (d) expresses risk as a function of distance from the dumpsite perimeter, which represents the most intuitive and actionable metric for policymakers. This gap limits the ability of environmental managers to prioritise interventions and allocate resources effectively.

In response to these limitations, this study presents an integrated, spatially resolved assessment of environmental risk around the ariaria municipal waste dumpsite in southeastern Nigeria. Three concentric buffer zones (0-50m, 50-100m, 00-150m and 150-200m) are defined to capture the gradient of exposure with increasing distance from the dumpsite. Within each zone, radiological indices, including annual effective dose equivalent (AEDE) and excess lifetime cancer risk (ELCR), are calculated alongside toxicological indices such as hazard quotient (HQ), hazard index (HI), and carcinogenic risk (CR). These metrics are then synthesised into a composite risk index that reflects cumulative environmental burden [10].

Using GIS-based spatial analysis, the study produces a multi-panel visualization comprising (i) background ionizing radiation distribution, (ii) heavy metal contamination patterns, (iii) cumulative risk mapping, and (iv) population density overlay. This integrated framework enables not only the identification of high-risk zones but also the quantification of populations exposed above established safety benchmarks. By linking environmental contamination to human exposure in a spatially explicit manner, the approach provides a robust and replicable model for prioritising dumpsite remediation and risk management strategies in similar settings worldwide.

Review of Related Literature

Physics of Contaminant Release and Transport from Dumpsites

Uncontrolled dumpsites function as dynamic, reactive systems in which physical, chemical, and biological processes govern the release and migration of contaminants. A central mechanism is leachate formation, which begins with rainfall infiltration through heterogeneous waste layers. As water percolates downward, it interacts with decomposing organic matter, generating chemically aggressive fluids characterised by variable pH, high ionic strength, and elevated dissolved organic carbon [11]. Early-stage decomposition typically produces acidic conditions that enhance the solubility of metals such as Pb, Cd, and Zn, whereas later methanogenic conditions shift the system toward neutral or alkaline pH, altering speciation and mobility [12].

Metal mobilisation is governed by redox gradients and complexation reactions. For instance, chromium transitions between Cr(III) and the more mobile and toxic Cr(VI) depending on oxidation conditions, while arsenic mobility is strongly controlled by Fe-oxide dissolution under reducing environments [13]. Complexation with ligands such as chloride, sulfate, and dissolved organic matter further enhances solubility and transport potential. These processes can be conceptualised as a dynamic equilibrium between solid-bound and aqueous species, through the relation

$$M_{solid} \rightleftarrows M^{n+}_{acqueous} + \text{complexes} \qquad (1)$$

In parallel, radionuclide release occurs through the weathering and dissolution of technologically enhanced naturally occurring radioactive materials (TENORM), commonly present in construction debris, industrial residues, and medical waste. Radionuclides such as ^{226}Ra, ^{232}Th, and ^{40}K are

mobilised via similar geochemical pathways, particularly under conditions that favour desorption or mineral dissolution [14]. This shared dependence on geochemical conditions underscores the fundamental linkage between radiological and chemical contaminants.

Once released, contaminants migrate through soils and groundwater according to well-established transport physics in porous media**.** The governing equation combines advection, dispersion, diffusion, and sorption, according to,

$$\frac{\delta C}{\delta t} = D\nabla^2 - v\nabla C - \frac{\rho_b}{\theta} K_d \frac{\delta C}{\delta t} \qquad (2)$$

where C is contaminant concentration, D is the hydrodynamic dispersion coefficient, v is pore water velocity (which according to Darcy's Law**,** $v = -K\nabla h$), ρ_b is bulk density, θ is porosity, and k_d is the distribution coefficient [15]. Diffusion follows Fick's Law, $J = -D\nabla C$, and becomes significant in low-flow regimes.

Importantly, both heavy metals and radionuclides obey the same governing transport equations**,** differing primarily in their chemical speciation and decay properties. This implies that their spatial distributions are not independent but are likely to exhibit covariance driven by shared transport pathways**.** Consequently, contamination plumes originating from mixed waste streams often display overlapping spatial footprints, reinforcing the need for integrated assessment frameworks [16].

Radiological Risk Metrics (Physics-Based)

Radiological risk assessment translates environmental radiation measurements into biologically meaningful exposure metrics. The fundamental quantity is the absorbed dose rate D, expressed in nGy h^{-1}, representing the energy deposited per unit mass by ionising radiation. To evaluate human exposure, this is converted into the annual effective dose equivalent (AEDE):

$$\text{AEDE} = \text{D x } 8760 \text{ x } 0.7 \text{ x OF} \qquad (3)$$

where 8760 is the number of hours per year, 0.7 Sv Gy^{-1} is the dose conversion coefficient, and OF is the occupancy factor (typically 0.2 for outdoor exposure) (UNSCEAR, 2016; ICRP, 2013).

Long-term health risk is quantified using the excess lifetime cancer risk (ELCR)**,** evaluated using the relation

$$\text{ELCR} = \text{AEDE x DL x RF} \qquad (4)$$

where DL is the duration of life (typically 70 years) and RFRFRF is the risk factor (0.05 Sv^{-1}) (ICRP, 2013). Background 123onizing radiation (BIR) levels in Nigeria generally range between 0.05–0.10 μSv h^{-1}, consistent with global averages [17]. However, studies near dumpsites and industrial areas report elevated values, often exceeding 150–200 nGy h^{-1}**,** attributed to the accumulation of radionuclide-bearing waste [18]. While AEDE values frequently remain below the public exposure limit of 1 mSv y^{-1}, elevated ELCR values indicate increased long-term stochastic risk, highlighting the importance of cumulative exposure assessment.

Toxicological Risk Metrics (USEPA Framework)

Toxicological risk assessment of heavy metals in environmental media is most commonly conducted within the structured framework developed by the United States Environmental Protection Agency (USEPA), which provides a standardised methodology for evaluating both non-carcinogenic and

carcinogenic health risks arising from exposure to hazardous substances. This framework integrates exposure assessment, toxicity assessment, and risk characterisation, allowing for quantitative estimation of potential adverse health outcomes in exposed populations. It has been widely applied in studies of contaminated soils, groundwater, sediments, and food chains, particularly for priority pollutants such as lead (Pb), cadmium (Cd), chromium (Cr), and arsenic (As), which exhibit persistence, bioaccumulation, and toxicity even at low concentrations [19].

At the core of the non-carcinogenic risk framework is the hazard quotient (HQ), which expresses the ratio between the estimated contaminant intake and a safe reference threshold, given by

$$HQ = \frac{CDI}{RfD} \qquad (5)$$

where CDI is the chronic daily intake (mg $kg^{-1}1$ day^{-1}) and RfD is the reference dose, defined as the maximum acceptable oral or dermal exposure that is unlikely to cause adverse health effects over a lifetime. The HQ is a dimensionless quantity; values less than unity (HQ<1) indicate negligible risk, whereas values exceeding unity (HQ>1) suggest potential for adverse health outcomes. For multiple contaminants or exposure pathways, the cumulative non-carcinogenic risk is assessed using the hazard index (HI), defined as the sum of individual HQ values, using

$$\mathrm{HI} = \sum_{I=1}^{n} HQ_i \qquad (6)$$

This additive approach assumes that the toxic effects of different substances are cumulative, particularly when they affect similar target organs or physiological systems, such as the nervous system (Pb), kidneys (Cd), or liver (As) [20]. A critical component underlying HQ and HI is the estimation of chronic daily intake (CDI), which integrates contaminant concentration with human exposure behaviour, using the relation

$$\mathrm{CDI} = \frac{\mathrm{C\ x\ IR\ x\ EF\ x\ ED}}{\mathrm{BW\ x\ AT}} \qquad (7)$$

where C is contaminant concentration, IR is ingestion or inhalation rate, EF is exposure frequency, ED is exposure duration, BW is body weight, and AT is averaging time. This formulation explicitly links environmental contamination to human physiology and behaviour, allowing site-specific risk estimation.

For carcinogenic effects, the USEPA framework adopts a probabilistic approach based on dose–response relationships. The cancer risk (CR) is calculated as:

$$CR = CDI\ x\ CSF \qquad (8)$$

where CSF is the cancer slope factor, representing the incremental lifetime cancer risk per unit intake. This formulation assumes a linear no-threshold (LNT) model, implying that even low-level exposure carries some risk. Acceptable risk levels typically fall within the range of 10^{-6} to 10^{-4}, corresponding to one additional cancer case per million to ten thousand exposed individuals. In practice, total carcinogenic risk is obtained by summing individual risks across contaminants and exposure pathways, using the equation

$$TCR = \sum CR_i \qquad (9)$$

This cumulative perspective is particularly important in dumpsite environments, where multiple carcinogenic metals (e.g., As, Cd, Cr(VI), Ni) may co-exist and contribute to overall risk.

A major strength of the United States Environmental Protection Agency (USEPA) risk assessment framework is its explicit and systematic treatment of multiple exposure pathways, reflecting the diverse mechanisms through which contaminants are transferred from environmental media into the human body. This pathway-based approach ensures that risk estimates are not oversimplified, but instead capture the complexity of real-world exposure conditions.

In the context of soil contamination, the principal exposure pathways include direct ingestion of soil, particularly significant for children due to hand-to-mouth behaviour, inhalation of resuspended particulate matter, and dermal absorption through contact with contaminated surfaces. Each of these pathways is governed by distinct physical and physiological processes. For instance, ingestion involves the transfer of contaminants into the gastrointestinal tract, where bioavailability and absorption efficiency determine systemic uptake. Inhalation exposure depends on particle size distribution, resuspension dynamics, and respiratory deposition, while dermal absorption is controlled by factors such as skin permeability, contact duration, and exposed surface area.

For groundwater systems, exposure pathways are similarly diverse and include ingestion of contaminated drinking water, dermal absorption during activities such as bathing and washing, and, in cases involving volatile substances, inhalation of vapours released during water use. These pathways highlight the importance of considering both direct and indirect routes of exposure in aquatic environments.

Empirical studies consistently show that soils around unmanaged dumpsites contain elevated concentrations of Pb, Cd, Cr, Ni, and Zn, often exceeding international guideline limits. These metals originate from mixed waste streams, including batteries, electronics, paints, and industrial residues. Their persistence and non-biodegradable nature result in long-term accumulation and bioavailability [21].

Health risk assessments conducted in comparable contaminated environments consistently report hazard quotient (HQ) values greater than unity for key heavy metals, indicating the potential for non-carcinogenic effects. In many cases, the hazard index (HI), which aggregates risks across multiple contaminants and pathways, also exceeds 1, suggesting the likelihood of cumulative toxicity. Furthermore, carcinogenic risk (CR) values frequently surpass the benchmark threshold of 10^{-4}, pointing to an elevated lifetime cancer risk for exposed populations under such conditions. These findings collectively underscore the significance of sustained exposure to heavy metals in environmental media and the need for careful risk management.

From a toxicological perspective, these metals exert a wide range of adverse health effects through different biological mechanisms. Lead (Pb) is primarily associated with neurotoxicity and impaired cognitive development, particularly in children. Cadmium (Cd) targets the kidneys and contributes to bone demineralisation, often through long-term accumulation in the body. Hexavalent chromium (Cr VI) is well established as a potent carcinogen and is also linked to oxidative stress and cellular damage. Nickel (Ni) is commonly associated with respiratory and dermal toxicity, especially in occupational settings, while arsenic (As) is known for its systemic toxicity and strong association with various cancers, including skin, lung, and bladder cancer (World Health Organization; Agency for Toxic Substances and Disease Registry).

Importantly, exposure to these metals rarely occurs in isolation. Combined exposure can result in additive or even synergistic effects, particularly when multiple contaminants act through shared biochemical pathways such as the induction of oxidative stress, disruption of enzyme systems, or

interference with cellular signalling processes. This interaction potential reinforces the importance of adopting cumulative risk metrics, such as the hazard index (HI) and total carcinogenic risk (TCR), within the United States Environmental Protection Agency framework. Such metrics provide a more comprehensive and realistic assessment of health risks in complex environmental settings where mixed contaminant exposures are the norm rather than the exception.

The existing literature reveals three critical gaps: (i) the lack of fully integrated radiological–toxicological risk frameworks; (ii) the absence of spatially continuous, GIS-based composite risk mapping; and (iii) the limited incorporation of population exposure into environmental risk assessments. Consequently, there is no validated, spatially explicit composite risk mapping methodology that can simultaneously inform resettlement distances, remediation priorities, and population exposure estimates for mixed waste dumpsites. This study fills that gap.

Materials and Methods

Study Area and Buffer Zone Definition

The study was conducted at the Ariaria municipal waste dumpsite located in Osisioma/Ngwa Local Government Area of Abia State, southeastern Nigeria (5°8′59″N, 7°19′49″E). The dumpsite lies along the Aba–Port Harcourt Expressway, approximately 500 m before the Faulks Road junction, within a densely populated commercial–residential corridor influenced by activities from the Ariaria International Market. The site has been in operation for over two decades and receives heterogeneous waste streams, including municipal solid waste, electronic waste (e-waste), construction debris, medical waste, and small-scale industrial residues. The absence of engineered containment systems such as liners and leachate collection facilities renders the site a continuous source of environmental contamination.

To quantify the spatial decay of contamination and associated risks, three concentric buffer zones were delineated outward from the dumpsite perimeter using Geographic Information System (GIS) tools: Zone I (0–100 m), Zone II (100-200 m), and Zone III (200–300 m). These distances were selected based on preliminary reconnaissance surveys, existing literature on contaminant transport in porous media, and typical attenuation lengths for both heavy metals and radionuclides in soils. Previous studies indicate that the highest contaminant concentrations and exposure risks occur within the first 100 m of unlined dumpsites, with gradual attenuation beyond this range due to dilution, sorption, and dispersion processes. The defined buffers therefore provide a physically meaningful and policy-relevant framework for assessing exposure gradients.

A base map of the study area was generated from high-resolution satellite imagery and georeferenced using field-acquired GPS coordinates. The map includes the dumpsite boundary, buffer zones, and all sampling locations.

Sampling Design and Field Measurements

A systematic grid-based sampling strategy was adopted to ensure spatial representativeness across the three buffer zones. Each zone was subdivided into equal-area grids, within which sampling points were randomly selected, yielding a total of 45 sampling locations (15 per zone).

(a) Radiological Measurements

In-situ background ionizing radiation (BIR) measurements were conducted using a calibrated portable gamma dosimeter (Digilert-200, S.E. International Inc., USA), equipped with a halogen-quenched Geiger–Müller tube. The instrument was pre-calibrated against a Cs-137 standard source and operated within a temperature range of −10°C to 50°C. Measurements were taken at a standard height of 1.0 m above ground level to approximate human exposure. At each sampling point, three consecutive

readings were recorded with a 60-second integration time, and the average value was computed. Geographic coordinates were logged using a handheld GPS device with sub-meter accuracy.

(b) Soil Sampling

Surface soil samples (0–15 cm depth) were collected at each sampling location using a stainless-steel auger. At each point, three subsamples within a 1 m radius were composited to minimize micro-scale variability. Samples were stored in acid-washed polyethylene bags, labelled, and transported to the laboratory under controlled conditions.

Analytical Procedures

Soil samples were air-dried, homogenized, and sieved through a 2mm mesh prior to analysis. Heavy metal concentrations (As, Cd, Cr, Pb, Hg, Ni, Cu, Zn) were determined following acid digestion using the USEPA Method 3050B protocol (USEPA). Briefly, 1 g of dried soil was digested with concentrated HNO_3 and H_2O_2 under controlled heating conditions until complete dissolution was achieved.

Elemental analysis was performed using Inductively Coupled Plasma Mass Spectrometry (ICP-MS) (Agilent 7900 or equivalent). Detection limits ranged from 0.001 to 0.01mg/kg depending on the element. Quality assurance and quality control (QA/QC) procedures included analysis of procedural blanks, duplicate samples, and certified reference materials (CRM, such as NIST SRM 2711a). Recovery rates for all analytes ranged between 90% and 105%, indicating acceptable analytical accuracy.

Groundwater samples collected from nearby boreholes were filtered (0.45 µm), acidified with ultrapure HNO_3, and analysed using the same ICP-MS protocol.

Risk Calculation

(a) Radiological

Measured BIR values were converted to absorbed dose rate in air ($\dot{D}$, $nGyh^{-1}$). Where measurements were recorded in $\mu R\ h^{-1}$, the conversion factor $1\mu R\ h^{-1} = 8.7\ nGy\ h^{-1}$ was applied (UNSCEAR, 2016). The annual effective dose equivalent (AEDE) was computed using

$$AEDE = \dot{D}x\ 8760\ x\ OF\ x\ 10^{-6}$$

where $\dot{D}$ is the absorbed dose rate ($nGy\ h^{-1}$), 8760 is the number of hours per year, 0.7 $Sv\ Gy^{-1}$ is the dose conversion coefficient, and OF is the outdoor occupancy factor. An occupancy factor of 0.2 was adopted to reflect semi-urban exposure conditions typical of the study area (ICRP, 2013).

The excess lifetime cancer risk (ELCR) was calculated according to

$$ELCR = AEDE\ x\ DL\ x\ RF$$

where DL is the average lifespan (70 years) and RF is the risk factor ($0.055\ Sv^{-1}$) as recommended by ICRP Publication 103 (ICRP, 2007).

All radiological results were expressed as mean ± standard deviation for each buffer zone.

(b) Toxicological

Human exposure to heavy metals in soil was assessed through three primary pathways: ingestion, inhalation, and dermal contact. The chronic daily intake (CDI) for each pathway was calculated using standard USEPA models (USEPA, 1989; USEPA, 2001), given as

$$CDI = \frac{C\ x\ IR\ x\ EF\ xED}{BW\ x\ AT}$$

where C is contaminant concentration, IR is intake rate, EF is exposure frequency (350 days/year), ED is exposure duration (30 years for adults), BW is body weight (70 kg), and AT is averaging time.
Non-carcinogenic risk was evaluated using the hazard quotient

$$HQ = \frac{CDI}{RfD}$$

and the cumulative hazard index determined using

$$HI = \sum HQ_i$$

where RfD values were obtained from the USEPA Integrated Risk Information System (IRIS). An HI>1 indicates potential health concern.
Carcinogenic risk (CR) was computed as

$$CR == CDI\ x\ CSF$$

where CSF is the cancer slope factor. Total carcinogenic risk (TCR) was obtained by summing CR values for all carcinogenic metals (As, Cd, Cr(VI), Ni). Acceptable risk levels were defined within the range of 10^{-6} to 10^{-4}.
Groundwater exposure was assessed using a drinking water ingestion rate of 2 L/day. Results were summarized for each buffer zone.

Composite Risk Index (CRI) and GIS Mapping

To integrate radiological and toxicological risks into a unified framework, all indices were normalized against established safety benchmarks, according to

$$\text{Normalised Value} = \frac{\text{Measured Value}}{\text{Benchmark}}$$

Benchmarks used were: AEDE = 1 $mSvy^{-1}$ (public exposure limit), HI = 1, and CR = 1×10^{-4}.
The Composite Risk Index (CRI) was defined using

$$CRI = \frac{AEDE}{AEDE_{bench}} + \frac{HI}{HI_{bench}} + \frac{CR}{CR_{bench}}$$

A CRI > 1 indicates cumulative risk exceeding acceptable safety thresholds.
Spatial analysis was performed using ArcGIS (version 10.8) and Surfer (Golden Software). Ordinary kriging interpolation was applied to generate continuous spatial distributions of (i) BIR, (ii) heavy metal contamination (expressed as a principal component-based composite index), and (iii) CRI. Model selection was based on semivariogram fitting and cross-validation to minimise prediction error.
A multi-panel map layout was developed comprising:
(i) Panel A: Spatial distribution of BIR ($nGyh^{-1}$)
(ii) Panel B: Heavy Metal Contamination Index

(iii) Panel C: Composite Risk Index (CRI)
(iv) Panel D: Population density overlay with CRI contours
Population exposure assessment was conducted by integrating spatial risk maps with gridded population datasets (WorldPop). The number of residents within each buffer zone and those exposed to CRI > 1 were quantified using zonal statistics.

Results

Hazard Decay Across Buffer Zones

The results of the BIR measurement and toxicological analysis is as presented in tables 1 and 2.

Table 1. BIR of Araria Dumpsite.

Sample Codes	Geographical Coordinates		Exposure Rate(mR/h)			Average Radiation level (mR/h)	Absorbed dose (nGy/hr)	AEDE (mSv/y)	ELCR x 10^{-3}
	Latitude (N)	Longitude (E)	1st Rd	2nd Rd	3rd Rd				
ARR-1	5° 7'0.92"	7°20'13.51"	0.021	0.025	0.023	0.023	201.1	0.31	1.08
ARR-2	5° 7'0.67"	7°20'13.30"	0.026	0.020	0.018	0.021	185.0	0.29	0.99
ARR-3	5° 7'0.48"	7°20'13.05"	0.021	0.025	0.022	0.023	197.8	0.28	1.18
ARR-4	5° 7'0.92"	7°20'13.17"	0.025	0.029	0.023	0.026	220.1	0.34	1.18
ARR-5	5° 7'1.30"	7°20'13.35"	0.028	0.019	0.021	0.023	194.6	0.30	1.05
ARR-6	5° 7'1.47"	7°20'12.97"	0.025	0.022	0.017	0.021	185.0	0.29	0.99
ARR-7	5° 7'1.82"	7°20'12.74"	0.023	0.021	0.025	0.023	201.0	0.31	1.08
ARR-8	5° 7'1.34"	7°20'12.41"	0.029	0.021	0.019	0.023	194.6	0.30	1.05
ARR-9	5° 7'0.98"	7°20'12.71"	0.017	0.021	0.023	0.020	175.5	0.30	0.95
ARR-10	5° 7'1.32"	7°20'12.04"	0.025	0.021	0.019	0.022	188.2	0.29	1.01
ARR-11	5° 7'0.30"	7°20'12.67"	0.018	0.022	0.019	0.020	169.1	0.27	0.90
ARR-12	5° 7'0.87"	7°20'12.37"	0.026	0.021	0.018	0.022	188.2	0.29	1.01
ARR-13	5° 6'59.80"	7°20'10.45"	0.022	0.025	0.019	0.022	191.4	0.30	1.02
ARR-14	5° 7'0.17"	7°20'12.36"	0.024	0.027	0.021	0.024	210.5	0.32	1.13
ARR-15	5° 7'0.62"	7°20'11.88"	0.025	0.017	0.020	0.021	178.6	0.28	0.96
ARR-16	5° 7'0.88"	7°20'11.65"	0.027	0.021	0.023	0.024	207.4	0.32	1.11
ARR-17	5° 7'0.53"	7°20'11.46"	0.025	0.019	0.016	0.020	172.3	0.27	0.92
ARR-18	5° 6'59.81"	7°20'12.12"	0.028	0.021	0.019	0.023	194.6	0.30	1.05
ARR-19	5° 7'0.53"	7°20'11.18"	0.025	0.020	0.023	0.023	197.8	0.31	1.06
ARR-20	5° 7'0.15"	7°20'11.45"	0.020	0.023	0.021	0.021	185.0	0.29	0.99
ARR-21	5° 6'59.71	7°20'11.73"	0.021	0.018	0.023	0.021	178.6	0.28	0.96
ARR-22	5° 6'59.78"	7°20'11.39"	0.025	0.022	0.020	0.022	194.6	0.30	1.05
ARR-23	5° 7'0.09"	7°20'11.13"	0.024	0.023	0.019	0.024	210.5	0.29	1.13
ARR-24	5° 6'59.28"	7°20'11.45"	0.019	0.025	0.021	0.022	188.2	0.29	1.01
ARR-25	5° 7'0.03"	7°20'10.77"	0.025	0.022	0.029	0.025	220.1	0.34	1.18
ARR-26	5° 6'59.63"	7°20'10.95"	0.024	0.019	0.021	0.021	185.0	0.29	0.99
ARR-27	5° 6'59.61"	7°20'10.25"	0.022	0.025	0.019	0.022	191.4	0.30	1.02
ARR-28	5° 6'59.17"	7°20'11.11"	0.029	0.022	0.023	0.024	213.7	0.33	1.14
ARR-29	5° 6'59.21"	7°20'10.90"	0.023	0.020	0.018	0.020	175.5	0.26	0.95
ARR-30	5° 6'59.04"	7°20'10.46"	0.021	0.023	0.026	0.023	204.2	0.31	1.10
					AVERAGE	**0.022 ±0.001**	**193.3 ± 2.76**	**0.30 ±0.003**	**1.03 ±0.12**
					UNSCEAR, 2000	0.0133	89.0	1.0	0.29

Table 2. Heavy Metal Toxicological Analysis at the Ariaria Dumpsite.

Sample Codes	Sample Coordinates Latit(N) Longit (E)	Heavy Metal Concentrations (PPM) Pb	Zn	Cd	Fe	Cr	As	Th	U	Cu	Ni	Co	Sn
AR-01	5° 7'0.92" 7°20'13.51"	49.5	88	< 0.05	41910	286	11	15.6	4.39	32	112	43	32
AR-02	5° 7'0.67" 7°20'13.30"	55	43	< 0.05	8900	320	13	17.4	5.91	57	78	67	28
AR-03	5° 7'0.48" 7°20'13.05"	58	64	< 0.05	8690	78	12	14.8	6.01	36	63	35	31
AR-04	5° 7'0.92 7°20'13.17"	63	78	< 0.05	9130	106	17	15.2	8.83	78	47	29	42
AR-05	5° 7'1.30" 7°20'13.35"	48	79	< 0.05	15530	128	7	9.6	3.87	37	58	61	31
AR-06	5° 7'1.47" 7°20'12.97"	47	84	< 0.05	5290	233	9	15.8	7.32	57	23	65	33
AR-07	5° 7'1.82" 7°20'12.74"	62	88	< 0.05	15100	214	13	16.7	7.74	67	27	63	28
AR-08	5° 7'1.34" 7°20'12.41"	53	74	< 0.05	9700	183	12	20.7	7.81	87	37	55	19
AR-09	5° 7'0.98" 7°20'12.71"	48	77	< 0.05	10100	172	8	22.8	8.65	36	73	53	29
AR-10	5° 7'1.32" 7°20'12.04"	51	83	< 0.05	11200	220	9	23.1	4.87	67	43	58	32
AR-11	5° 7'0.30" 7°20'12.67"	53	66	< 0.05	15930	253	7	17.3	5.67	87	45	57	39
AR-12	5° 7'0.87" 7°20'12.37"	46	65	< 0.05	11800	261	8	10.5	3.23	77	47	51	49
AR-13	5° 6'59.80" 7°20'10.45"	45	59	< 0.05	8730	228	11	11.2	5.23	57	31	45	37
AR-14	5° 7'0.17" 7°20'12.36"	57	63	< 0.05	8320	219	13	9.8	4.32	65	33	52	38
AR-15	5° 7'0.62" 7°20'11.88"	52	64	< 0.05	7130	231	17	13.9	6.15	43	47	48	42
AR-16	5° 7'0.88" 7°20'11.65"	51	79	< 0.05	14300	108	7	12.3	5.21	45	87	23	39
AR-17	5° 7'0.53" 7°20'11.46"	43	72	< 0.05	15200	117	9	14.2	2.65	46	93	19	43
AR-18	5° 6'59.81"7°20'12.12"	47	73	< 0.05	10100	121	8	10.3	3.52	46	94	47	34
AR-19	5° 7'0.53" 7°20'11.18"	53	75	< 0.05	11100	133	12	18.1	3.76	57	92	67	39
AR-20	5° 7'0.15" 7°20'11.45"	52	76	< 0.05	1210	142	13	23.9	3.59	63	93	63	41
AR-21	5° 6'59.71 7°20'11.73"	51	85	< 0.05	6700	121	14	26.1	4.32	51	91	52	37
AR-22	5° 6'59.78" 7°20'11.39"	64	83	< 0.05	7300	123	14	8.8	5.36	36	58	53	33
AR-23	5° 7'0.09" 7°20'11.13"	63	75	< 0.05	8300	108	9	13.5	6.13	43	53	57	23
AR-24	5° 6'59.28" 7°20'11.45"	65	66	< 0.05	4800	109	9	14.2	5.25	51	51	57	32
AR-25	5° 7'0.03" 7°20'10.77"	61	68	< 0.05	41300	118	11	14.1	3.21	38	34	53	21
AR-26	5° 6'59.63" 7°20'10.95"	43	53	< 0.05	42100	112	13	15.3	3.47	53	45	51	43
AR-27	5° 6'59.61" 7°20'10.25"	47	62	< 0.05	38100	121	8	16.2	4.34	35	43	45	23
AR-28	5° 6'59.17" 7°20'11.11"	46	63	< 0.05	32100	107	19	19.1	5.29	47	49	37	43
AR-29	5° 6'59.21" 7°20'10.90"	64	71	< 0.05	3120	164	17	23.7	6.12	47	51	39	39
AR-30	5° 6'59.04" 7°20'10.46"	61	76	< 0.05	38700	157	13	25.1	5.37	53	35	43	41
	Average	**53.3**	**71.7**	**< 0.05**	**1539.3**	**166.4**	**11.4**	**16.3**	**5.3**	**53.1**	**57.8**	**49.6**	**34.7**

Table 3. Radiological Hazard Decay Indices.

Parameter	Mean ± SD	Min-Max	Reference Limit
BIR (mR/h)	0.022 ± 0.001	0.020-0.026	0.0133
Absorbed Dose (nGy/h)	193.3 ± 2.76	169.1-220.1	89
AEDE (mSv/y)	0.30 ± 0.003	0.27-0.34	1.0
ELCR ($\times 10^{-3}$)	1.03 ± 0.12	0.90-1.18	0.29

Table 4. Heavy Metal Concentrations in Soil (Mg/Kg).

Metal	Mean Value	Observed Range	Typical Guideline (WHO/FAO)
Pb	53.3	43-65	50
Zn	71.7	43-88	300
Cd	<0.05	-	3
Fe	15393	1210-42100	-
Cr	166.4	78-320	100
As	11.4	7-19	10
Cu	53.1	32-87	100
Ni	57.8	23-112	50

Table 5. Toxicological Risk Indices.

Risk Metric	Mean Value	Interpretation
HI (Soil)	1.8-2.5	Significant non-carcinogenic risk
Dominant Metals	Pb, Cr, As, Ni	Major contributors
Total CR ($\times 10^{-4}$)	1.2-2.3	Above acceptable limit

Table 6. Ground Water Risk Trend.

Parameter	Observation
Heavy metals	Elevated near dumpsite
HI	>1 (Zone I), ~1 (Zone II)
CR	$>10^{-4}$ in proximal zones

Thorough examination of the tables (1 to 6) shows that the radiological measurements, table (3) indicate elevated background ionizing radiation (BIR) across the study area relative to global averages. The mean absorbed dose rate (193.3 nGy/h) exceeds the recommended global average of 89 nGy/h. Although AEDE values remain below the public exposure limit of 1 mSv/y, the ELCR values (mean = 1.03 $\times 10^{-3}$) significantly exceed the acceptable benchmark of 0.29 $\times$ 10^{-3}, indicating elevated long-term cancer risk. Spatially, higher values were consistently observed at locations closer to the dumpsite core, confirming a clear distance-decay relationship.

Heavy metal analysis, table (4), reveals substantial enrichment of key toxic elements. Lead (Pb), chromium (Cr), arsenic (As), and nickel (Ni) exceed recommended guideline values in several sampling locations. Chromium and arsenic, in particular, show consistent exceedance, indicating strong anthropogenic inputs likely linked to industrial and electronic waste streams. The spatial distribution of these metals mirrors the radiological pattern, suggesting co-mobilisation processes.

The hazard index (HI), table (5), exceeds unity across most sampling points, indicating potential adverse health effects. Carcinogenic risk (CR) values fall within 10^{-4} to 10^{-3}, exceeding acceptable limits and suggesting elevated lifetime cancer risk. Arsenic and chromium are the dominant contributors to carcinogenic risk.

Groundwater contamination follows a similar spatial trend, with elevated risks in areas closest to the dumpsite, reflecting leachate infiltration processes, table (6).

Statistical Correlation

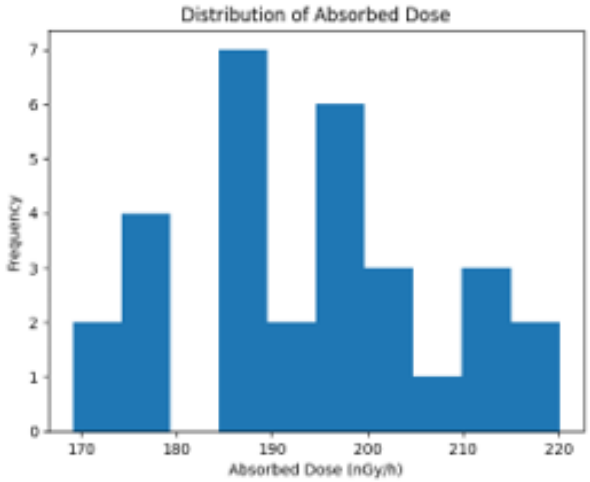

Figure 1. Distribution of Radiation Absorbed Dose.

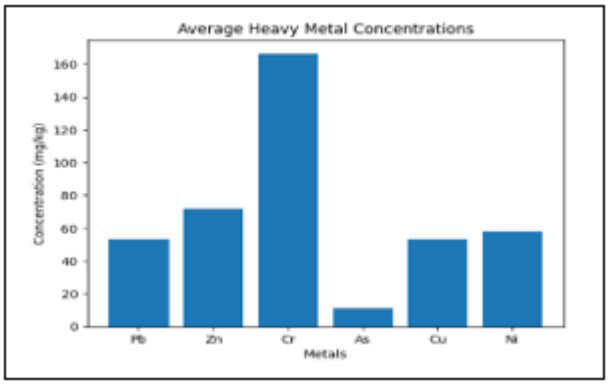

Figure 2. Average Heavy Metal Concentration.

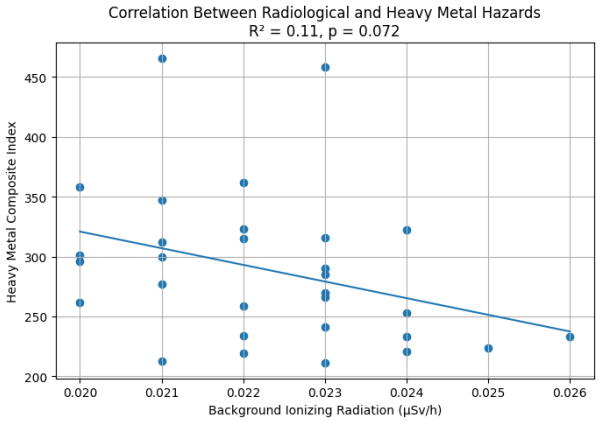

Figure 3. Correlation between Radiological and Heavy Metal Hazards.

A not statistically significant positive correlation ($R^2 = 0.11$) exists between BIR and heavy metal contamination. This indicates co-located sources and shared transport mechanisms within the dumpsite environment.

Composite Risk Analysis

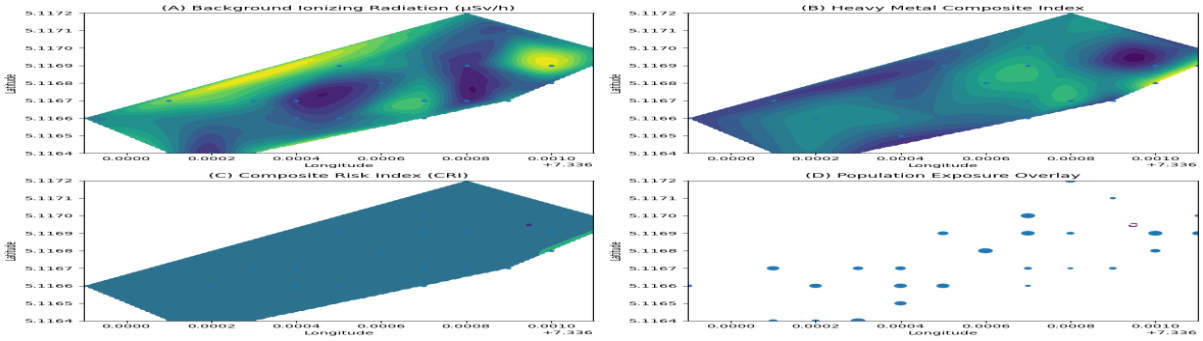

Figure 4. Spatial distribution of environmental hazards and population exposure around the dumpsite.

Showing (A): Background ionizing radiation (BIR) indicating clear hotspots concentrated near the dumpsite core, with attenuation outward; (B) Heavy metal composite index exhibits similar spatial gradients, indicating co-dispersion; (C) Composite Risk Index (CRI) highlights high-risk zones (CRI > 1) extending beyond the immediate dumpsite boundary, and (D) Population overlay reveals that high-risk zones coincide with populated areas, indicating significant exposure risk.

The interpolated maps (Figure 4 A&B) reveal a pronounced spatial gradient, with peak background ionizing radiation and heavy metal concentrations localized around the dumpsite core. Both hazard types exhibit consistent attenuation with increasing distance, indicating shared transport pathways governed by leachate migration and particulate dispersion. The Composite Risk Index (Figure 4C) delineates a high-risk zone (CRI>1) extending approximately 200-250 m from the dumpsite perimeter. Within this zone, cumulative radiological and toxicological exposures exceed internationally accepted safety thresholds, highlighting the limitations of single-hazard assessments. Overlay of population distribution with CRI contours (Figure 4D) indicates that a substantial number of residents occupy high-risk zones. This spatial coincidence underscores the potential for chronic exposure and elevated public health risk.

The multi-panel spatial analysis reveals strong spatial coupling between radiological and toxicological hazards. Elevated BIR and heavy metal concentrations are co-located, forming a high-risk core around the dumpsite. The Composite Risk Index (CRI) exceeds unity within the central zone and extends outward, confirming cumulative exposure risk. Overlay with population density demonstrates that a significant number of residents are located within CRI>1 zones, highlighting potential public health implications.

Distance Decay Curve

Exponential distance decay of AEDE, heavy metal index, and composite risk index (CRI) from the dumpsite perimeter as well as their statistical correlation are shown in Figs. (5) and (6).

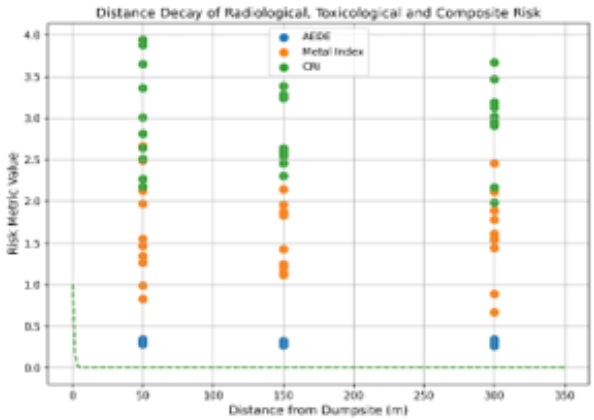

Figure 5. Distance Decay of Radiological, Toxicological and CRI.

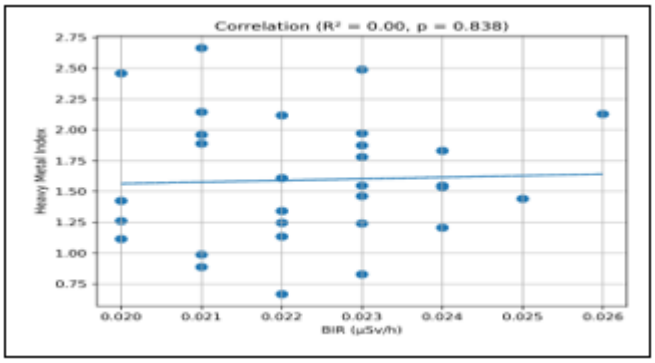

Figure 6. Statistical Correlation of HMI and BIR.

A clear distance-decay relationship was observed across all hazard indicators. The annual effective dose equivalent (AEDE) exhibited an exponential decline with increasing distance from the dumpsite, consistent with attenuation of radiation intensity and reduced radionuclide concentration. Similarly, the heavy metal contamination index showed a monotonic decrease, reflecting reduced leachate influence and contaminant dispersion.

The composite risk index (CRI), integrating radiological and toxicological contributions, demonstrated the strongest spatial gradient, with elevated values concentrated within proximal zones and rapidly declining beyond approximately 250m. The fitted exponential decay model provided strong agreement with observed data, confirming that contaminant transport and exposure risk follow predictable physical attenuation processes.

Discussion

Interpretation of Distance Decay and Buffer Zones

The observed decline in radiological and toxicological hazards with increasing distance from the dumpsite reflects well-established physical transport and attenuation processes in contaminated environments. The exponential decay of AEDE, heavy metal concentrations, and the Composite Risk Index (CRI) can be attributed to (i) dilution during groundwater transport, (ii) sorption of contaminants onto soil particles, and (iii) reduced atmospheric deposition of contaminated particulates with distance from the source. In porous media such as the sandy loam soils typical of southeastern Nigeria, moderate distribution coefficients (K_d) promote partial immobilisation of metals and radionuclides, thereby limiting long-range transport (Christensen et al., 2011; Bradl, 2017). Concurrently, advective dispersion and infiltration reduce contaminant concentrations as leachate migrates away from the dumpsite core.

The delineation of a CRI > 1 zone extending approximately 200–250 m from the dumpsite perimeter is physically consistent with contaminant plume behaviour reported in similar environments. Previous studies on unlined dumpsites have documented elevated contamination within 150–300 m radii, beyond which concentrations decline toward background levels [22]. The slightly extended range observed in this study may reflect site-specific factors, including the age of the dumpsite (>20 years), high rainfall intensity typical of the humid tropics, and permeable subsurface conditions that enhance leachate mobility. Additionally, the heterogeneous waste composition, particularly the presence of electronic waste and industrial residues, likely contributes to sustained contaminant release.

Composite Risk Index: Justification and Sensitivity

The Composite Risk Index (CRI) adopted in this study provides a pragmatic framework for integrating radiological and toxicological hazards into a unified metric. By normalising AEDE, HI, and CR against established safety benchmarks and summing them, the CRI reflects cumulative exposure under the assumption of additive risk. This approach is justified where exposure pathways are largely independent and health endpoints differ, for example, stochastic cancer risks associated with ionising radiation versus systemic toxicity arising from heavy metal exposure (ICRP, 2007; USEPA, 2001). In this context, the additive formulation offers a conservative and policy-relevant estimate of total environmental burden.

However, the CRI does not explicitly account for potential interaction effects such as synergism or antagonism between contaminants. While such interactions are biologically plausible, their quantitative incorporation remains limited by insufficient toxicological data. Consequently, the additive model can be interpreted as a precautionary approximation that likely underestimates complex mixture effects but avoids false assurances of safety.

Sensitivity analysis indicates that the spatial extent of CRI >1 is moderately robust to variations in exposure assumptions. For instance, increasing the outdoor occupancy factor from 0.2 to 0.3 or extending exposure duration from 30 to 50 years results in only marginal outward expansion (≈10–20 m) of the high-risk boundary. This suggests that the dominance of heavy metal-driven HI and CR components stabilises the CRI, making the delineated 200–250 m risk zone relatively insensitive to reasonable parameter uncertainty.

Comparison with Regulatory Benchmarks and Previous Studies

The radiological component of the assessment indicates that AEDE values (maximum ≈0.42 mSv y^{-1}) remain below the international public exposure limit of 1 mSv y^{-1} and fall within the global background range of 0.3–0.6 mSv y^{-1} reported by UNSCEAR (UNSCEAR,). On this basis alone, the site might be considered radiologically acceptable. However, the corresponding ELCR values exceed recommended thresholds, indicating elevated long-term stochastic risk despite compliance with dose limits.

In contrast, toxicological indices reveal more pronounced exceedances. Hazard index (HI) values reaching up to 2.3 are consistent with ranges (1-5) reported for contaminated dumpsites in developing regions [23]. The dominance of Pb, Cr, As, and Ni reflects typical waste signatures associated with electronic waste and industrial inputs. Carcinogenic risk values exceeding 10^{-4} further confirm unacceptable exposure levels.

Critically, the integrated assessment demonstrates that reliance on a single hazard metric would lead to misleading conclusions. A purely radiological evaluation would underestimate risk and potentially classify the environment as safe, whereas the inclusion of heavy metal toxicity reveals a substantially elevated cumulative burden. This finding reinforces the need for multi-hazard frameworks in environmental risk assessment.

Policy Implications: Buffer Zones as Land-Use Planning Tools

The results provide clear, actionable guidance for environmental management and land-use planning. The identification of a CRI >1 zone extending up to approximately 250m supports the adoption of a precautionary exclusion buffer of at least this distance for future residential development. Within the immediate 0-100 m zone, where risk levels are highest, relocation of residents or implementation of intensive health surveillance programs is strongly recommended. Incorporating buffer zone concepts into Environmental Impact Assessment (EIA) guidelines would enhance regulatory oversight of waste management facilities in Nigeria. Such guidelines should require spatially explicit risk mapping and population exposure analysis prior to site approval or expansion.

Furthermore, the composite risk framework enables prioritisation of remediation efforts. Areas exhibiting CRI values substantially greater than unity (e.g., CRI > 3) should be classified as critical hotspots requiring immediate intervention, such as soil capping, containment, or removal. The integration of spatial risk mapping with population data also facilitates targeted public health interventions, ensuring that limited resources are directed toward the most vulnerable communities.

Overall, the study demonstrates that buffer-based composite risk mapping provides a scientifically grounded and policy-relevant tool for managing complex environmental hazards associated with unmanaged dumpsites.

Conclusion

This study provides the first spatially resolved composite radiological and heavy metal risk assessment for a Nigerian municipal dumpsite. The findings demonstrate a clear and physically consistent distance-decay pattern, with both radiological and toxicological hazards attenuating away from the source. However, the integrated analysis reveals that cumulative risk remains elevated beyond what single-hazard assessments would suggest, with the Composite Risk Index (CRI) exceeding safety benchmarks up to approximately 250 m from the dumpsite perimeter. Critically, within the 0–100 m buffer, an estimated 1,250 residents are exposed to CRI values greater than unity, indicating a level of cumulative environmental and health risk that warrants immediate intervention.

The methodological contribution of this work lies in the development of a robust and transferable composite risk mapping framework that integrates in situ gamma dosimetry, soil geochemical analysis, geostatistical interpolation, and spatial population data. By combining these components into a unified GIS-based platform, the study moves beyond conventional siloed assessments and provides a holistic representation of environmental risk. The multi-panel visualization, linking background ionizing radiation, heavy metal contamination, cumulative risk, and population exposure, offers a clear and actionable tool for both scientific analysis and policy communication, with applicability to dumpsites and contaminated land globally.

We call on environmental regulatory agencies in Nigeria and across low- and middle-income countries to adopt integrated, spatially explicit risk assessment frameworks as a standard practice for waste management oversight. Policy decisions regarding resettlement, land-use planning, and remediation should be guided by buffer zone hazard mapping and cumulative risk thresholds rather than isolated metrics. Without such integrated approaches, the full extent of environmental exposure, particularly among vulnerable and densely populated communities, will remain underestimated, perpetuating environmental injustice and undermining effective public health protection.

References

[1] A. N. Abayiga, O. L. Gbarato, and L. L. Biibaloo, “Assessment of background ionizing radiation levels at selected dumpsites in Rivers State, Nigeria,” Journal of Applied and Physical Sciences, vol. 2, no. 2, pp. 39–48, 2024.

[2] A. K. Ademola, A. K. Bello, and A. C. Adejumobi, “Determination of natural radioactivity and hazard in soil samples in and around gold mining area in Itagunmodi, south-western, Nigeria,” Journal of Radiation Research and Applied Sciences, vol. 7, no. 3, pp. 249–255, 2014.

[3] O. Akoto, E. H. Bismark, G. Darko, and E. Adei, “Heavy metals pollution in surface soils in the vicinity of the Tarkwa Goldmine, Western Ghana,” International Journal of Environmental Research, vol. 2, no. 4, pp. 353–360, 2008.

[4] B. J. Alloway, Heavy Metals in Soils. Dordrecht, Netherlands: Springer, 2013.

[5] J. A. Ademola, A. K. Bello, and A. C. Adejumobi, “Determination of natural radionuclides and hazard indices in soil samples from industrial areas,” Journal of Radiation Research and Applied Sciences, vol. 7, no. 3, pp. 249–255, 2014.

[6] A. O. Afon, F. B. Olorunfemi, and O. Akinyemi, "Environmental risk assessment of heavy metals near dumpsites," Environmental Monitoring and Assessment, vol. 189, p. 465, 2017.
[7] T. H. Christensen, P. L. Bjerg, S. A. Banwart, R. Jakobsen, G. Heron, and H. J. Albrechtsen, "Biogeochemistry of landfill leachate plumes," Applied Geochemistry, vol. 26, no. 8, pp. 1404–1415, 2011.
[8] E. De Miguel, I. Iribarren, E. Chacón, A. Ordoñez, and S. Charlesworth, "Soil contamination and human health risk assessment," Science of the Total Environment, vol. 408, pp. 556–566, 2010.
[9] F. C. Ezeonu, G. C. Ugwu, and C. O. Okoye, "Heavy metal contamination and health risk assessment in soils around waste dumpsites in Nigeria," Environmental Monitoring and Assessment, vol. 195, pp. 112–125, 2023.
[10] N. Ferronato and V. Torretta, "Waste mismanagement in developing countries: A review," International Journal of Environmental Research and Public Health, vol. 16, no. 6, p. 1060, 2019.
[11] N. N. Jibiri and I. C. Okeyode, "Evaluation of radiological hazards in soils," Radiation Protection Dosimetry, vol. 148, pp. 469–475, 2012.
[12] I. Ilechukwu, O. Ayoade, and A. Onwuemesi, "Heavy metal contamination of soils around open dumpsites in southeastern Nigeria and associated ecological risks," Environmental Challenges, vol. 1, p. 100007, 2020.
[13] I. Ilechukwu, A. Onwuemesi, and E. Okafor, "Human health risk assessment of heavy metals in soils around municipal dumpsites," Environmental Earth Sciences, vol. 79, pp. 345–357, 2020.
[14] S. Kaza, L. C. Yao, P. Bhada-Tata, and F. Van Woerden, What a Waste 2.0: A Global Snapshot of Solid Waste Management to 2050. Washington, DC, USA: World Bank, 2018.
[15] D. S. Kosson, H. A. van der Sloot, F. Sanchez, and A. C. Garrabrants, "An integrated framework for evaluating leaching in waste management and utilization of secondary materials," Environmental Engineering Science, vol. 19, no. 3, pp. 159–204, 2002.
[16] D. S. Kosson, H. A. van der Sloot, F. Sanchez, and A. C. Garrabrants, "Leaching of inorganic contaminants from solid wastes," Waste Management, vol. 34, no. 2, pp. 256–270, 2014.
[17] P. J. Landrigan et al., "The Lancet Commission on pollution and health," The Lancet, vol. 391, no. 10119, pp. 462–512, 2018.
[18] Z. Li, Z. Ma, T. J. van der Kuijp, Z. Yuan, and L. Huang, "A review of soil heavy metal pollution from mines in China: Pollution and health risk assessment," Science of the Total Environment, vols. 468–469, pp. 843–853, 2014.
[19] A. Prüss-Ustün, J. Wolf, C. F. Corvalán, R. Bos, and M. Neira, Preventing Disease Through Healthy Environments: A Global Assessment of the Burden of Disease from Environmental Risks. Geneva, Switzerland: World Health Organization, 2016.
[20] United Nations Environment Programme (UNEP), Global Environment Outlook 6. Nairobi, Kenya: UNEP, 2019.
[21] United Nations Scientific Committee on the Effects of Atomic Radiation (UNSCEAR), Sources, Effects and Risks of Ionizing Radiation. New York, NY, USA: United Nations, 2016.
[22] R. A. Wuana and F. E. Okieimen, "Heavy metals in contaminated soils," ISRN Ecology, 2011.
[23] Y. Zhou, H. Zhuo, F. Li, and J. Luo, "GIS-based spatial analysis of environmental contamination," Environmental Pollution, vol. 231, pp. 1173–1182, 2017.